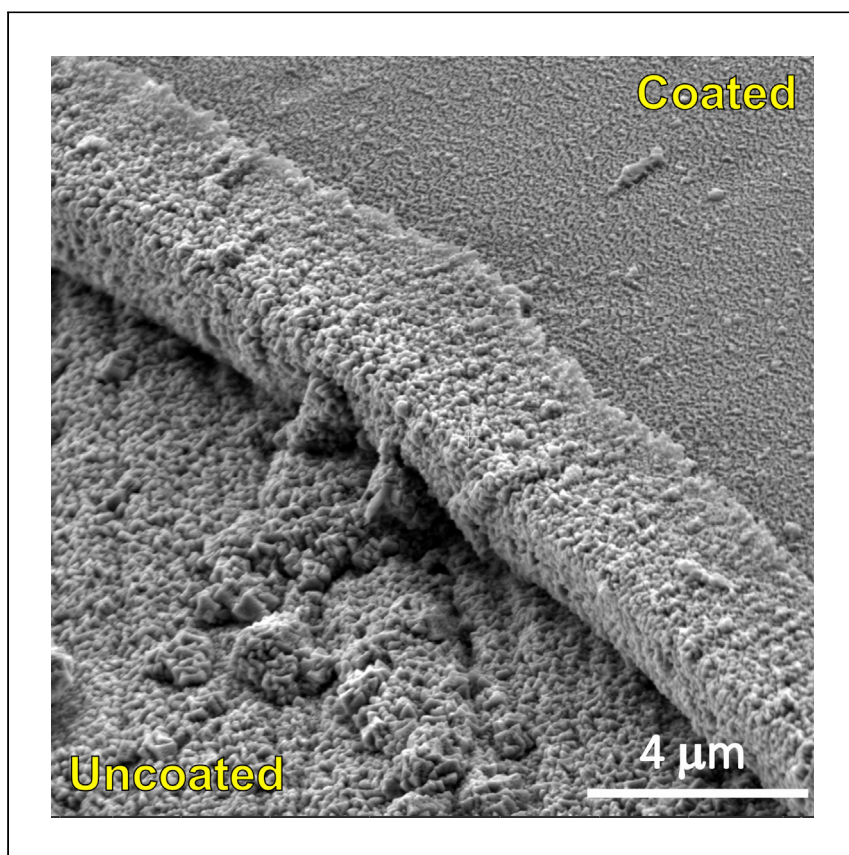


Article

Slippery omniphobic covalently attached liquid coatings mitigate carbon deposition by autoxidation of jet fuel



Siavash Khodakarami, Hanyang Zhao, Kazi Fazle Rabbi, Qiyuan Wu, Jingcheng Ma, Nenad Miljkovic

nmiljkov@illinois.edu

Highlights

Hybrid low surface energy and smooth coating for carbon deposition mitigation

Scalable coating methodology applicable for complex heat exchangers

Reduced jet fuel autoxidation by reduction of metal surface catalytic effects

Comparison with jet fuel fouling on copper, stainless steel, and alumina

The autoxidation of jet fuel results in carbon deposition on metals. Khodakarami et al. use a scalable hybrid coating to combine SiO₂ and a slippery omniphobic covalently attached liquid to mitigate carbon deposition by eliminating the interface between the fuel and substrate and to provide a low surface energy smooth interface.

Article

Slippery omniphobic covalently attached liquid coatings mitigate carbon deposition by autoxidation of jet fuel

Siavash Khodakarami,^{1,5} Hanyang Zhao,^{1,5} Kazi Fazle Rabbi,¹ Qiyuan Wu,¹ Jingcheng Ma,¹ and Nenad Miljkovic^{1,2,3,4,6,*}

SUMMARY

The decomposition of jet fuel at elevated temperatures leads to fuel fouling and deposit formation on metallic walls. Here, we develop and study an innovative sol-gel silicon dioxide (SiO₂) hybrid anti-fouling coating to mitigate fuel fouling. Our coating has low surface roughness (<1 nm) and low surface energy (<12 mJ/m²), reducing the heterogeneous nucleation rate during deposition. The sol-gel SiO₂, which forms the base coating, further minimizes exposure of the metal substrate to the fuel, which can act as a catalyst and increase the decomposition reaction rate. We tested the fouling behavior in a custom-built fuel fouling test loop. Tests were able to characterize the efficacy of our coatings and to benchmark performance with bare copper, stainless steel, and Inconel 600 metals as well as commercial anti-fouling coatings, such as alumina and SilcoTek. Our coating demonstrated reduced fouling rates of at least 96% when compared with bare samples.

INTRODUCTION

The majority of aircraft are powered by petroleum distillate. The chemical structure of commercial jet fuel is based on kerosene, a middle distillate product of the crude oil refinery process. In some aircraft, this jet fuel can also be used as a coolant before it is used to power the aircraft due to its high heat capacity and presence during the mission profile.¹ However, jet fuel at elevated temperatures can decompose due to a variety of mechanisms.^{2,3} Decomposition not only affects the heat exchange inside the thermal management system rejecting heat to the fuel, but also other components such as engine injector nozzles.⁴ One of the most common and simplest methods to limit fuel decomposition is to limit the maximum wetted wall temperature of the components, which come into direct contact with the fuel. In the case of the fuel-to-fluid heat exchanger, which couples the fuel to the coolant circulating in the aircraft, the fuel-side of the heat exchanger is designed such that the maximum wetted wall temperature does not exceed 200°C. Limiting the fuel-side maximum wetted wall temperature necessitates the increase in heat exchanger area (A). Increasing the area results in higher heat exchanger mass and volume, a harsh but mandatory limitation for aviation platforms.

Carbon deposition at elevated temperatures can be separated into two regimes. The autoxidation reaction happens between 150°C and 350°C, where deoxygenated fuel shows a much lower carbon deposition rate than oxygenated fuel.⁵ The pyrolysis regime generally happens when temperatures exceed 450°C, where the fuel will experience decomposition, cyclization, and condensation into a deposit

¹Department of Mechanical Science and Engineering, University of Illinois at Urbana-Champaign, Urbana, IL 61801, USA

²Department of Electrical and Computer Engineering, University of Illinois at Urbana-Champaign, Urbana, IL 61801, USA

³Materials Research Laboratory, University of Illinois, Urbana, IL 61801, USA

⁴International Institute for Carbon Neutral Energy Research (WPI-I2CNER), Kyushu University, 744 Motooka, Nishi-ku, Fukuoka 819-0395, Japan

⁵These authors contributed equally

⁶Lead contact

*Correspondence: nmiljkov@illinois.edu
<https://doi.org/10.1016/j.xcrp.2022.100859>

morphology. Dissolved oxygen plays a major role in the deposition rate in the pyrolysis regime. Between 350°C and 450°C, the transient regime is established where the chemical reaction is very complex and not well understood.⁶

The mechanism of carbon deposition due to the autoxidation reaction is well studied and has been experimentally investigated to understand the cracking and deposition behavior of jet fuel at elevated heat loads.^{5,7} Detailed methodologies and standards have been developed to ensure consistency of jet fuel testing results within this regime.^{8,9} Exposed metal and dissolved metal in the fuel can significantly increase the autoxidation reaction rate.^{10,11} For example, dissolved copper compounds with concentrations as low as 1.3 ppb can increase the oxidation rate by 58%.¹² Many studies have investigated the mechanisms that govern metal catalytic behavior during the fuel autoxidation reaction.^{13,14} Others have reported the effect of alternate metals such as manganese and iron in fuel oxidation.^{15,16} In general, three main methods to achieve jet fuel fouling reduction exist. The first one is deoxygenation, which mainly targets the autoxidation reaction. Deoxygenation is typically achieved by membrane separation or chemical processing.^{17–19} The second method is to stabilize the jet fuel by additional refining to either remove some of the unstable compounds, such as heteroatomic compounds or polar species,^{20,21} or to add more thermally stable compounds.^{22,23} The third, and most popular and well-studied method, is to add chemical additives to stabilize the fuel at elevated temperatures and thus reduce fouling. Chemical additives are widely used in the aviation and defense industries. Several successful commercialized products exist that can be added to the jet fuel^{8,24} or integrated into the system in the form of a coating.²⁵

Here, in an attempt to eliminate the needs for additives, and to further increase the allowable maximum wetted wall temperature, we develop an innovative hybrid slippery omniphobic covalently attached liquid (SOCAL) coating, which not only blocks soluble oxidized product transport from the metal substrate but also reduces the fouling rate. By utilizing a base sol-gel silicon dioxide (SiO₂) coating, followed by SOCAL functionalization, the hybrid coating eliminates contact between fuel and substrate, reducing the catalytic metal compound-mediated reaction rate. Although the autoxidation reaction cannot be completely eliminated due to dissolved oxygen, our hybrid SOCAL coating limits the formation of carbon deposits via its low surface roughness, low surface energy, and resulting low foulant-surface adhesion. These three properties of our hybrid SOCAL coating make it a broad anti-fouling strategy, even for deposits stemming from pyrolysis. To quantify the fuel fouling behavior, we developed an experimental test facility to characterize internal-channel flow fouling of Jet-A1 (kerosene) jet fuel in accordance with guidelines provided by the jet fuel thermal oxidation test (JFTOT). Comparison of coated copper (Cu) and stainless steel (SS 304) tube samples with their bare (uncoated) counterparts was conducted. The results revealed a 96% reduction in carbon deposition on Cu after coating the Cu tube internal surface with our hybrid SOCAL coating. We then compared the fuel fouling performance on other materials, including alumina ceramic, Inconel 600, and a commercially available coating (SilcoKlean). Our hybrid SOCAL coating shows comparable or better performance and is more cost-effective and widely applicable to a variety of base materials. Overall, our proposed hybrid SOCAL coating presents a facile method to achieve fuel fouling mitigation, in addition to reduction of insoluble particle formation and surface exposure. Our method not only shows high effectiveness in the autoxidation fouling regime, it has the potential to be exploited in the pyrolysis regime for other petroleum distillate products in a variety of applications.



Figure 1. Optical images of the cross-sectioned tube samples before and after the fuel fouling experiment

(A–F) Samples shown include (A) bare uncoated Cu, (B) hybrid SOCAL-coated Cu, (C) bare uncoated SS 304, (D) hybrid SOCAL-coated SS 304, (E) SilcoKlean 1000-coated SS 304, and (F) bare uncoated Inconel 600. The coated samples showed obvious qualitative visual advantage in reducing jet fuel deposition when compared with the uncoated samples. Images of the pre-test and tested samples have been stitched together in the mid-point of the figure to enable ease of comparison. The images are taken from an area located in the middle (axial dimension) of the tubes.

RESULTS AND DISCUSSION

Focused ion beam milling analysis of jet fuel fouling experiment

Carbon deposition on the samples after each experiment was determined to be very thin ($<10\ \mu\text{m}$) as the mass difference before and after the experiments, as measured by a sensitive microbalance (AS 82/220.R2, Radwag), was very small. The small change in mass made the measurement of additional mass deposition difficult to realize. To overcome this challenge, we cut the sample open along the axis of flow and cut them into small 1 cm long pieces along the flow direction. Direct optical observation of the tube insides revealed very distinct differences between the bare and coated samples. Optical images of all the samples are shown in Figure 1. The bare uncoated Cu and SS samples showed very obvious carbon deposition via the formation of a dark layer on the tube inside (tested column in Figure 1). The Cu tube was smooth and reflective before testing (Figure 1A, pre-test), ending up uniformly coated with carbon deposits after the test (Figure 1A, tested). The SS tube had an uneven surface (Figure 1C, pre-test), hence the carbon deposition distribution was not as uniform (Figure 1C, tested). Spots of the underlying metal substrate could be observed in some locations. For the Cu sample coated with the hybrid SOCAL coating (Figure 1B, pre-test), the base metal was well preserved after testing (Figure 1B, tested), with very few spots of carbon deposition. The hybrid SOCAL coating appears to be very smooth and uniform. Similar results were observed on the hybrid SOCAL-coated SS tube (Figure 1D), with no obvious carbon deposition observed. Figure 1E shows a tested SS tube sample coated with the SilcoKlean commercial coating, demonstrating good fouling resistance. The SilcoKlean coating had a different color when compared with the hybrid SOCAL coating, with the surface

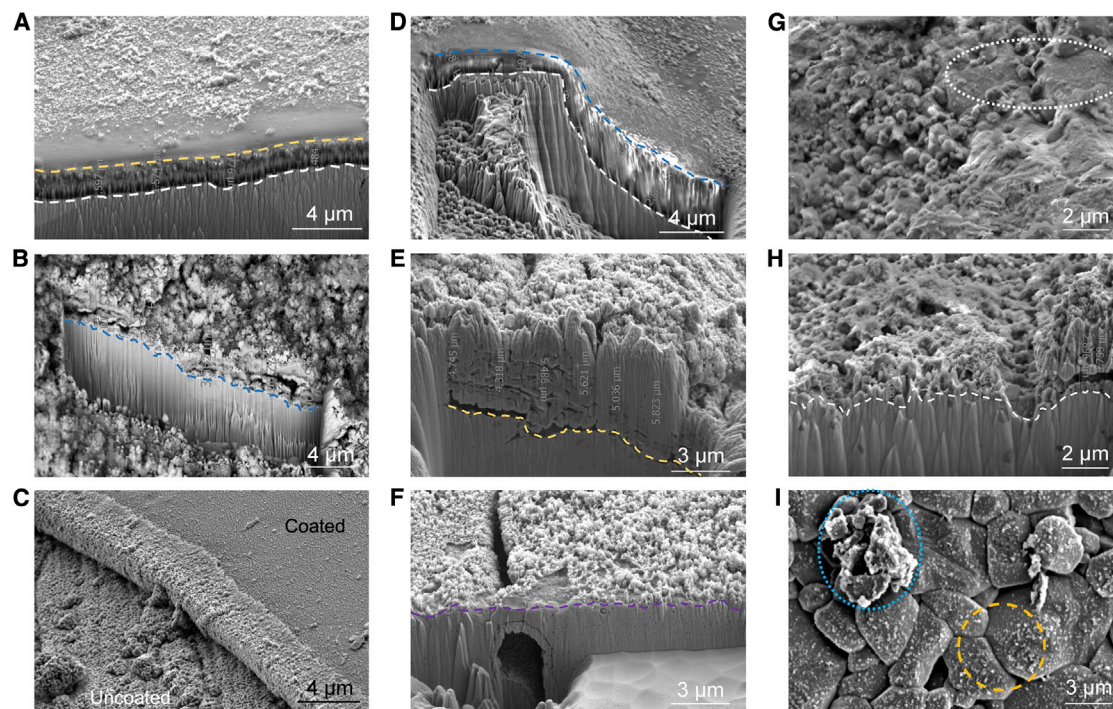


Figure 2. Scanning electron microscopy images of the FIB-milled regions

(A) Hybrid SOCAL-coated Cu tube. The yellow and white dotted lines represent the SOCAL-deposit interface and the Cu-SiO₂ interface, respectively. (B) Uncoated Cu tube after fuel fouling experiment. The blue dotted line represents the Cu-deposit interface. The thickness of the carbon deposition on the uncoated sample is $4.4 \pm 0.54 \mu\text{m}$, and the hybrid SOCAL-coated sample is $0.17 \pm 0.05 \mu\text{m}$. (C) SEM image of carbon deposition on a sample that was half coated with the hybrid SOCAL coating. The bottom left region is the uncoated Cu, while the top right region is the hybrid SOCAL-coated Cu. (D) SEM images of FIB-milled sections on the hybrid SOCAL-coated SS 304 tube. The blue and white dotted lines represent the SOCAL-deposit interface and the SS-SiO₂ interface, respectively. (E) Uncoated SS 304 counterpart after conducting the fuel fouling experiments. The thickness of carbon deposition on the uncoated sample was $5.18 \pm 0.53 \mu\text{m}$ and the hybrid SOCAL-coated sample was $0.17 \pm 0.05 \mu\text{m}$. The yellow dotted line represents the SS-deposit interface. (F) FIB section view of the SS 304 sample coated with the commercially available SilcoKlean anti-coking coating after jet fuel fouling experiments. The effective thickness of the carbon deposit on the SilcoKlean coating was $0.32 \pm 0.10 \mu\text{m}$. The purple dotted line represents SilcoKlean-deposit interface. (G) Angled-view FIB-milled cross-section of the Inconel 600 sample after fuel fouling tests. (H) FIB-milled cross-section of the Inconel 600 sample after fuel fouling tests. The dotted white circle shows the exposed area of Inconel 600 substrate. The dashed white line represents the Inconel 600-deposit interface. The thickness of the carbon deposition on the Inconel 600 sample was estimated to be $1.76 \pm 0.96 \mu\text{m}$. (I) SEM top-view image of the alumina ceramic tube after fuel fouling testing. The blue dotted circle and yellow dashed-dotted circle outline the thick and sparse deposit morphologies, respectively, observed on alumina.

having a duller finish, potentially indicating more carbon deposition than the hybrid SOCAL coating. The uncoated Inconel 600 tube (Figure 1F, pre-test) had better performance when compared with uncoated Cu and SS. However, traces of carbon deposition were still observed (Figure 1F, tested).

Optical images obtained from cutting the tubes provided qualitative information about the carbon deposition (Figure 1). When the tubes were cut open, the internal side of the tubes looked the same in any azimuthal location, indicating that sedimentation was not observed. To further analyze the carbon deposition quantitatively, we utilized focused ion beam (FIB) milling to measure the thickness of the carbon deposit. Figure 2 shows FIB milling results for the bare uncoated Cu sample as well as the hybrid SOCAL-coated Cu sample after a fuel fouling test was conducted. The Cu sample having the hybrid SOCAL coating showed a very clear layer of sol-gel SiO₂, having a thickness of $2.03 \pm 0.09 \mu\text{m}$ (Figure 2A). On top of the coating,

randomly distributed particles were found, indicating that carbon deposition was minimal and sparse (Figure 2A). The thickness of these observed particles could not be measured as they did not form a continuous layer. To estimate the thickness, we used ImageJ. The average deposition thickness was estimated using ten independent and spatially distinct measurement on the FIB-milled scanning electron microscopy (SEM) images. The thickness uncertainty was calculated by taking the standard deviation of these measurements. The estimated average size of the carbon deposit was 387 ± 107 nm. We then used ImageJ to process the surface density of the carbon deposition and the measured surface coverage was 43.6%. With these quantitative pieces of information, we estimated the effective thickness of the carbon deposition to be approximately 0.17 ± 0.05 μm . The fouling rate reduction on the coated sample was then estimated by comparing the effective thickness of the carbon deposit between the coated and uncoated samples (knowing the experiment duration) by using FIB milling analysis after the experiments are conducted. For a detailed breakdown of the method used to estimate the effective thickness, with data reduction methodology, please see Note S1 and Figure S1.

For the uncoated Cu sample (Figure 2B), the thickness of the carbon deposition was measured to be 4.4 ± 0.54 μm . The deposition thickness was approximately 26 \times larger when compared with the hybrid SOCAL-coated Cu sample (Figure 2A). Figure 2C showed a carefully fabricated half-coated Cu sample after conducting the fuel fouling experiment. The step observed in Figure 2C running from top-left to bottom-right marks the line differentiating the coated and uncoated Cu sides. Partial coating was implemented by only dipping half of the tube (~ 10 cm) inside the solution and then reversing the movement direction using the controlled dip-coating setup to avoid coating the other half of the tube (the remaining 10 cm). Figure 2C reveals that the uncoated side was covered with thick carbon deposition, while the coated side was clean and with few deposit aggregations. This image analysis further verifies the conclusions obtained from Figures 2A and 2B.

The SS 304 bare sample and the hybrid SOCAL-coated sample showed similar jet fuel fouling test result as those of the Cu tube (Figures 2D and 2E). One major difference was that the SS sample had uneven inner walls before testing, with some spots having sharp edges. The hybrid SOCAL coating was able to cover the uneven substrate and create a smooth surface, resulting in a non-uniform thickness of the hybrid SOCAL coating (Figure 2D). The carbon deposition appears to have the same qualitative pattern as observed on the hybrid SOCAL-coated Cu sample. Since carbon deposits could not achieve full surface coverage by the end of the test, the same aforementioned analysis was used to estimate the thickness of carbon deposition on the SS 304 sample. The average size of carbon deposit particles was 419 ± 128 nm, with a surface coverage of 39.7%, resulting in an effective carbon deposition thickness of 0.17 ± 0.05 μm . For the bare uncoated SS 304 sample (Figure 2E), the carbon deposition thickness was 5.18 ± 0.53 μm . The results clearly show that the hybrid SOCAL sample has a clear advantage over the uncoated surface, demonstrating a 97% fuel fouling reduction on SS 304 substrate. Uncertainties in the measurements represent the standard deviation of the 10 measurements on each surface.

Figure 2F shows the SS 304 sample coated with the commercially available SilcoKlean 1000 anti-coking coating after conducting the fuel fouling experiments. Top-view SEM imaging showed many trenches on the coating, with the top surface nearly fully covered by carbon deposition. The ion-milled side view of the SilcoKlean-coated Cu surface (Figure 2F) showed that the deposition had a similar pattern as observed on the hybrid SOCAL sample (Figure 2D), mainly in the form

Table 1. Summary of estimated effective carbon deposition thickness on all tested samples

	Cu bare	Cu SOCAL	SS bare	SS SOCAL	SS SilcoKlean	Inconel 600	Alumina ceramic
Thickness (μm)	4.4 ± 0.54	0.17 ± 0.05	5.18 ± 0.53	0.17 ± 0.05	0.32 ± 0.10	0.22 ± 0.12	0.21 ± 0.07

of nanoparticles. The main differences were: (1) the hybrid SOCAL coating showed a smaller surface coverage, whereas the SilcoKlean 1000 showed almost full surface coverage with carbon deposition. (2) The nanoparticles were larger on the SilcoKlean 1000 coating. The same method was used to estimate the coating thickness as that used on the hybrid SOCAL-coated samples. For the SilcoKlean-coated Cu sample, the average particle size was 493 ± 157 nm with a surface coverage of 64.5%. Hence, the effective thickness of carbon deposition on the SilcoKlean-coated Cu sample was 0.32 ± 0.10 μm .

Figures 2G and 2H show fuel fouling result after FIB milling and cross-sectioning of the Inconel 600 and alumina ceramic tubes. Similar to what was observed in the optical images (Figure 1), parts of the Inconel 600 substrate were covered by carbon deposition. Other areas showed exposed substrate (white dotted circle in Figure 2G) and were covered by nano particles with sizes ranging from 300 to 700 nm. The average particlesize was 545 ± 103 nm. The areas covered with nano particle deposition appeared brighter when viewed by optical means. The areas that were fully covered with carbon deposition appear darker (black spots) when viewed optically (Figure 1). To estimate the thickness of the carbon deposition, the dark and bright areas were calculated separately and combined together. The dark area had an average thickness of 1.76 ± 0.96 μm . The surface coverage of the nanoparticle deposition (bright area) was 58.4%. The overall dark area ratio was 6.7%, hence the effective thickness calculated by combining the two areas was 0.22 ± 0.12 μm .

Figure 4I shows SEM images of fuel fouling result on the alumina ceramic tube. Note that the dotted blue circle and dashed-dotted yellow circle show two different patterns of carbon deposition. The carbon deposits enclosed in the blue dashed circle are very similar to those observed on the Cu and SS 304 samples coated with the hybrid SOCAL coating. Only part of the surface was coated with carbon deposition, with large ceramic areas exposed. The size of these deposits is also very small. The yellow dashed-dotted circle encloses a large amorphous carbon deposit. These large deposits are sparse and can be observed on the surface when inspected under SEM. The larger deposits grow on top of areas where two ceramic crystals meet, demonstrating the importance of having a smooth surface to prevent fouling. Areas on top of the ceramic crystal perform similarly to hybrid SOCAL-coated Cu and SS 304 hybrid SOCAL-coated samples, while areas between two ceramic crystals performed poorly at preventing fouling. We estimated the thickness of carbon deposition by measuring the average particle size, which was 570 ± 192 nm with a 64% surface coverage, demonstrating an effective thickness of 0.21 ± 0.07 μm . A summary of all samples and the associated effective thickness of carbon deposition after jet fuel fouling tests is shown in Table 1.

X-ray photoelectron spectroscopy analysis of jet fuel fouling experiments

In addition to FIB milling analysis to determine the carbon deposition thickness, we utilized X-ray photoelectron spectroscopy (XPS) to investigate the composition of the carbon deposition. The only tube having an almost full carbon deposition coverage, as observed with a detected Cu atom percentage of <3%, was the uncoated Cu tube. For the purpose of consistency, all samples analyzed using XPS

Table 2. Elemental ratio obtained by XPS for the tested bare Cu, tested hybrid SOCAL-coated Cu, and pre-test hybrid SOCAL-coated Cu

Sample	Element	Area (survey)	Ratio (survey)	Area (fine)	Ratio (fine)
Cu bare	C	13,757.29	63.75	8,554.5	60.6
	O	22,919.78	36.25	16,313.4	39.4
Cu SOCAL tested	C	13,237.61	58.8	7,815.2	55.3
	O	17,243.13	26.14	12,021.1	29.0
	Si	2,769.64	15.06	1,803.8	15.6
Cu SOCAL clean	C	13,367.79	32.87	11,079.5	41.1
	O	43,083.69	36.15	27,538.2	34.8
	Si	10,292.7	30.98	5,319.8	24.1

Both the ratio calculated for the survey and fine scans is reported.

were Cu tubes. To compare the effect of carbon deposition on the hybrid SOCAL coating, we also tested a freshly coated hybrid SOCAL coating without conducting fuel fouling experiments. The composition information calculated by survey and fine scans for each element are shown in Table 2, with the survey results of each sample shown in Figure 3. For the bare Cu sample, no Cu signal can be detected due to the coverage of the surface with a thick carbon layer. On the hybrid SOCAL protected Cu surface, the silicon signal can be identified, showing that the SOCAL layer remains exposed on the surface after jet fuel fouling, which is consistent with the FIB result. We attempted to develop an understanding of the chemistry of the deposited carbon layer. However, previous studies have already reported that the carbon formed by fuel fouling can exist in many forms of aromatic hydrocarbons,²⁶ which are difficult to distinguish from each other from the C1s spectrum. Therefore, we cannot specify the detailed chemistry of the carbon layer. However, it can be determined that the carbon layer is composed of hydrocarbon chains (main peak at ~285 eV) and conjugated aromatic structures (shake-up signals that are centered about 6–7 eV higher than the main carbon peak and are generally broad), which is consistent with previous reports.²⁷ The C1s spectrum of tested bare Cu can be found in Figure S2.

Fouling reduction mechanism of the interfaces

As shown in past studies, dissolved metal compounds within the fuel can dramatically increase the autoxidation reaction rate. This principle has been used for creating anti-coking coatings for hydrocarbon fuels. Among the available coatings, metal organic chemical vapor deposition (MOCVD) alumina is commonly used and has been reported to have a 68% reduction in fuel fouling deposition when compared with uncoated tubes.²⁸ The experiments were conducted at much higher temperatures of 575°C, where the effect of metal catalysis is more important.^{29,30} In our work, the alumina ceramic material is superior when compared with the uncoated metals tested. It showed a 96% reduction in carbon deposition when compared with the bare SS sample. Alumina is reported to have a very low surface energy, with quantitative results varying according to the size of the crystallites. Forms of θ -alumina have been shown to have negative surface energy,³¹ which is key as surface energy plays an important role in fouling.^{32,33} Although the majority of past literature examining surface energy and roughness effects have focused on salt scaling on metallic surfaces,^{32,34} the fundamental mechanistic principles governing anti-scaling behavior of salts and those of carbon deposition are analogous. The theory governing both deposition mechanisms is classical nucleation theory, which states that the combination of a smooth surface with a low surface energy can dramatically reduce scaling.³⁵ The past work on scaling, along with the fact that alumina was proven to have the ability to mitigate fuel fouling and coking, broaden the selection criteria for fuel fouling.

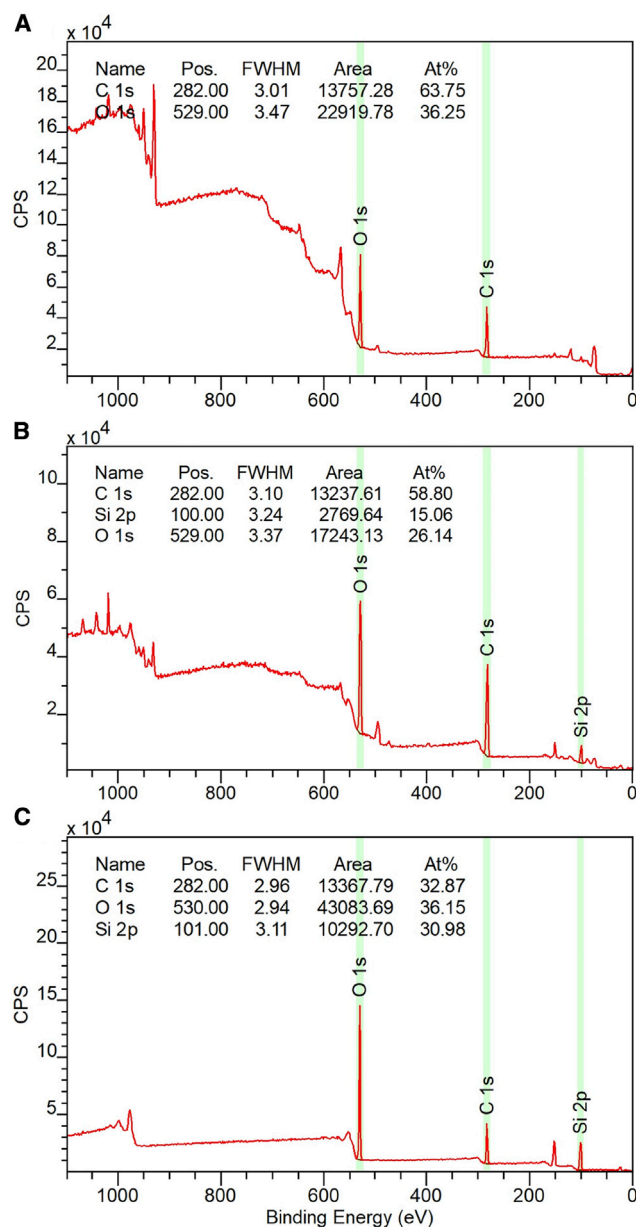


Figure 3. XPS survey result on coated Cu tube samples

(A) Tested bare Cu.

(B) Tested hybrid SOCAL-coated Cu.

(C) Clean and un-tested hybrid SOCAL-coated Cu.

The hybrid SOCAL coating developed and tested here has similar properties as alumina. Both have low surface energy, and both physically separate the metal surface from the jet fuel. Although MOCVD methods for coating alumina produce rough surfaces and cracks,²⁸ the sol-gel prepared SiO₂ coating used in the hybrid SOCAL coating is both smooth and uniform.³⁴ Hence, the promising results demonstrated for the fuel fouling reduction on the hybrid SOCAL coating are not surprising.

The surface chemistry of common metals limits the attachment of SOCAL directly on metallic surfaces. Hence, the sol-gel SiO₂ is needed to enable covalent bonding of

SOCAL to the surface. Furthermore, deposition of SOCAL directly on metal would not reduce the roughness of the substrate, which is achieved through the thicker sol-gel SiO₂ deposition. This is the second important role the sol-gel layer plays in reducing the foulant nucleation site density. Sol-gel SiO₂ also protects the substrate from exposure to the jet fuel. A thin SOCAL coating has a much higher chance of establishing pinholes in it when compared with the thicker hybrid coating.³⁴ Therefore, the hybrid coating is more effective at corrosion protection compared with SOCAL alone. Although alternate methods of SiO₂ deposition, such as physical vapor deposition and chemical vapor deposition (CVD), have potential, the advantage of the sol-gel method is its high scalability, which allows for cost-effective coating of large-scale and complex geometries such as heat exchangers. In addition, the smoothness of the hybrid SOCAL coating caused uniform foulant deposition at small length scales, while the alumina surface showed larger depositions at several spots (Figure 2I). The low contact angle hysteresis of SOCAL is also a measure of chemical homogeneity of the surface, which is decoupled from the surface energy and more related to defect density required for foulant nucleation. For example, it is possible to achieve low contact angle hysteresis on a hydrophilic surface with high chemical homogeneity.³⁶ The 97% fouling reduction when compared with uncoated SS 304 tubes demonstrates even lower carbon deposition when compared with alumina ceramic tube samples.

Both ceramic and hybrid SOCAL coatings eliminate the interface formed between the substrate and jet fuel. Therefore, the autoxidation reaction should be identical for both cases. The kinetic model for nucleation rate of heterogeneous nucleation suggests smaller surface energy is favorable for reduced nucleation rate.³⁷ The measured surface energy of the sol-gel SiO₂ is 30.3 ± 1.3 mJ/m². The surface energy is further reduced to 11.17 ± 1.51 mJ/m² on the SOCAL coating, which is two orders of magnitude smaller than the bare metallic surface (e.g., Cu and SS 304).^{38,39} Another important parameter governing fouling rate is the surface roughness. It has been shown that surface roughness affects scaling tendency by increasing nucleation sites and adhesion strength of deposited scale.⁴⁰ The root-mean-square roughness of the sol-gel coating is $R_q = 0.9$ nm, which is 96.25% lower than the roughness of polished Cu (= 24 nm).³⁴ The surface-science-based roughness for the SOCAL coating is $r = 1.001$, where r is defined as the total surface area of the sample normalized by the projected surface area of the sample. The surface of the ceramic tube is rough with many crystallites (Figure 2I). The peaks and valleys act as nucleation sites and can ensure the growth of larger particle deposition in conjunction with smaller particles. However, on the hybrid SOCAL coating for both the Cu and SS 304 tubes, the deposited carbon particles were uniformly small in size (<1 μm).

The coating first acts as a barrier to eliminate the interface between the jet fuel and metallic substrate. This helps to reduce catalytic effects of the substrate on the fouling rate. However, autoxidation eventually occurs at pinholes or even without the presence of the substrate, with insoluble products formed in the bulk jet fuel. After particles are formed, the coating minimizes the deposition rate. Both the low surface roughness and low surface energy are required to minimize deposition. To better differentiate the effect that roughness and surface energy play on carbon deposition, fouling experiments were conducted on a Cu tube coated with only the sol-gel SiO₂ coating (see Figures S3 and S4). The average carbon deposition thickness on the sol-gel SiO₂ coating was 0.71 ± 0.07 μm, larger than the value corresponding to the hybrid SOCAL coating (0.17 ± 0.05 μm). However, the measured deposition thickness was much smaller than the carbon thickness on the uncoated Cu surface (4.4 ± 0.54 μm). Decoupling of the effects of possible chemical reactions,

which aid in autoxidation, is more difficult to achieve as the SiO₂ coating devoid of SOCAL simply removes the effect of surface energy, but cannot decouple the effect of roughness from the effect of preventing the jet fuel from contacting the metallic wall (substrate).

As an alternative material, polydimethylsiloxane-based (PDMS) coatings can also reduce the surface energy and the droplet contact angle hysteresis of bare metal surfaces. The surface energy of PDMS is generally higher than 20 mJ/m²,^{41,42} resulting in lower thermodynamic energy barriers for foulant nucleation from insoluble particles caused by autoxidation, as well as higher foulant-substrate adhesion after deposition. In addition to surface energy, roughness of the coating plays a very important role in minimizing the nucleation sites for the foulant, as well as the apparent adhesion of the foulant to the surface. Grafting PDMS directly onto the metal substrate may not fully cover the micrometric topographical asperities on the substrate, which are common for the majority of engineering materials. However, the intermediate layer in the hybrid coating provides an atomically smooth interface, thus performing better when compared with grafting molecular chains of PDMS on to bare metal surfaces. Quasi liquid-like PDMS-coated surfaces have been recently investigated for low-temperature liquid repellency, anti-icing, and condensation applications at moderate temperatures.^{43–47} These PDMS chemistries are generally stable up to 150°C,⁴⁸ and more studies and investigations are required for long-term high-temperature application as well as durability of the PDMS-based coatings.

A similar analysis can be made on the SilcoKlean 1000 coating for the SS 304 tube. The surface is coated with SiO₂, which has a high surface energy (52 mJ/m²).³³ The high surface energy affects the anti-fouling performance. On the other hand, the surface of the coating is also rough. These two factors help to ensure that the fuel fouling deposition on the commercially coated SilcoKlean 1000 SS 304 tube is higher when compared with the hybrid SOCAL-coated and alumina ceramic tubes.

The three bare metal samples show the expected results. For bare Cu and SS 304, a very thick and dense carbon deposition covered the surface after conducting the fuel fouling test. This deposition can be verified both by optical imaging (Figure 1) and electron microscopy (Figure 2). On the SS 304 sample, the optical images show few depositions with smaller surface coverage due to the uneven surface of the tube. The carbon deposition filled the valleys but does not reach the top of the roughness features. Studies have been conducted on fuel fouling behavior on the surface of various iron- and nickel-based alloy in the past,^{29,49,50} with conclusions varying based on test conditions. Past studies have focused on the transient or pyrolysis regimes due to a focus on coking deposition mitigation. Coking is a very common byproduct of the pyrolysis reaction and has been reported to be catalyzed by iron and nickel. State-of-the-art anti-coking coatings include alumina, SiC, and others.⁵¹ Tests conducted under 350°C and a 500 psig pressure show that SS 304 has approximately a 28% lower carbon deposition rate when compared with Inconel 600. However, our tests showed the opposite conclusion. The Inconel 600 showed approximately a 96% reduced deposition thickness when compared with the uncoated SS 304. The contradicting results show the complexity of the fuel autoxidation reaction. This may be because the catalyst efficiency is different for nickel and iron in the autoxidation regime. The SS 304 tube has a 69% Fe content and a 10% Ni content. Inconel 600 has an 8% Fe content and a 74% Ni content. Additional studies are needed to better understand the mechanisms governing the chemical catalyst pathways for nickel and iron in the autoxidation reaction. The reduced deposition rate on Inconel 600 is due to the pre-oxidation of the surface, which limits the

exposure of the jet fuel to the catalytic metallic surface.⁵⁰ Additional studies are required to fully understand this phenomenon.

To analyze the composition of the coating and the carbon deposition, we utilized XPS to measure the C, Si, and O surface content on three different samples. The uncoated Cu tube sample showed full coverage with carbon deposition and was used to analyze the deposition composition. The result (Figure 3A) showed a 36.25% oxygen content and a 63.75% carbon content. Other miscellaneous elements, such as sulfur and nitrides, appear in the XPS data. This result is close to what has been reported in past studies.⁵² Past work has also analyzed a different standard jet fuel PR-3 and the test arrangement was different. These two reasons, in addition to the complex composition of kerosene itself, can explain the small difference in reported oxygen percentage between our work and past studies. Figures 3B and 3C show the ratio between C, O, and Si before and after the experiment for the hybrid SOCAL-coated sample. The change in silicon ratio can be understood by considering that parts of the coating surface are covered by the carbon deposition, which only has carbon and oxygen. Based on this, a simple calculation can be done by comparing silicon ratio to estimate the coverage of the carbon deposition, which is 44.3%. The silicon ratio used here is the average between the survey and the fine scan. Here, we assumed that the fully clean surface (pre-test) corresponds to the average silicon content in the survey and fine scan (27.5%). Taking the ratio of the silicon content (averaged over survey and fine scan) of the surface after the test to the pre-test value corresponds to the undeposited area ($15.3/27.5 = 0.5564$). Therefore, the remaining area, which is 44.3% of the surface, would be covered with deposits. This result is very close to the 43.6% obtained using SEM image analysis. When assuming that the covered area has the same composition as the carbon deposits, and the uncovered area has the same composition as a clean hybrid SOCAL coating, we can then use the surface coverage to calculate the C and O ratios, which are 50.7% and 34.9%, respectively. This result agrees well with the XPS scan results (average between survey and fine scan) for the hybrid SOCAL sample, which show 57% and 27.6%, respectively. The small difference arises because of potential morphological changes of the SOCAL coating at high heat loads (jet fuel fouling testing). Furthermore, both the SEM and XPS analysis only scan a very small fraction of the entire tube sample, with some systematic error inevitable in the analysis.

Thermal performance and durability

The use of a thin hybrid SOCAL layer ($\sim 2 \mu\text{m}$) minimizes the additional parasitic thermal resistance associated with the coating.⁵³ The thermal resistances associated with the Cu tube wall, the SS 304 wall, and the hybrid coating are 0.27 mK/W, 6.32 mK/W, and 0.11 mK/W, respectively. The thermal resistance of the coating is much smaller than the thermal resistances associated with the tube walls. Hence, the hybrid coating plays a negligible effect on the overall thermal performance of the heat exchanger. In fact, the overall heat transfer coefficient of the system is reduced by less than 1% for conservative conditions using highly turbulent external flow (see Note S3 and Table S5).

Reducing the fouling rate inside the heat exchanger increases the long-term thermal performance and lifetime of the heat exchanger, which further reduces the maintenance and associated labor costs.^{54,55} Furthermore, the fabrication process of the hybrid SOCAL is scalable to large-scale surfaces as it does not require any vacuum system or high-temperature process. The coating is solution based and is deposited by a dip-coating procedure, which is controlled by a linear motor to ensure constant dipping and withdrawal velocity (Figure 4). After the tube samples were coated, they

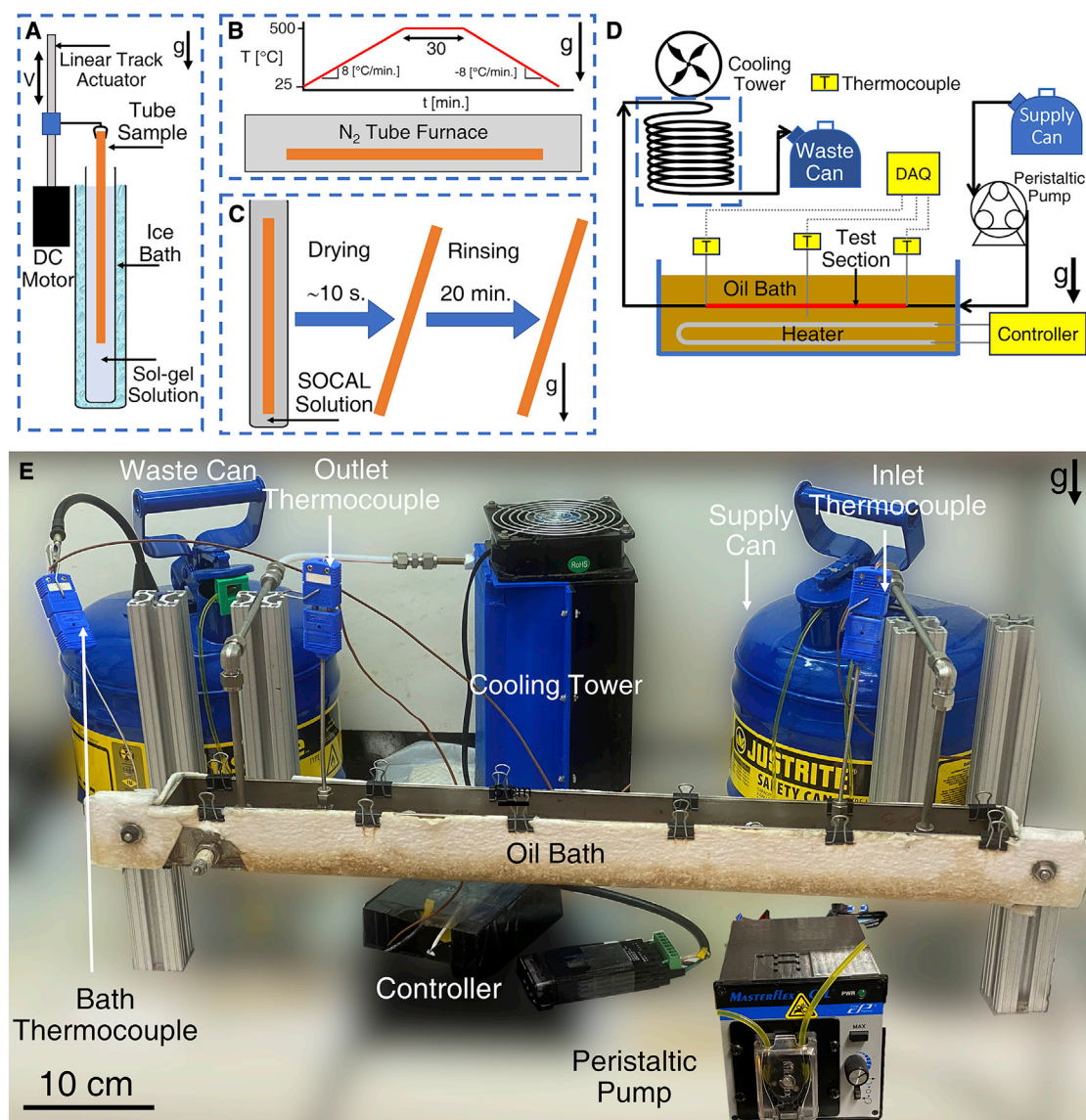


Figure 4. Coating method and experimental facility

(A) Schematic of dip coating of the sol-gel SiO₂ coating.

(B) Sintering of the sol-gel coating. The inset shows the tube furnace heating ramp rate and hold times for the sintering process of the sol-gel coating.

(C) Dip coating of the SOCAL coating.

(D) Schematic of the fuel fouling experimental setup. Schematic not to scale. An immersive heater and a proportional integral differential controller were used to maintain the bulk temperature of the silicone oil bath. A custom-made cooling tower was used to reduce the heated fuel temperature to ensure that the fuel waste was stored at a safe temperature.

(E) Photograph of the experiment setup.

were mounted to the test section of the jet fuel fouling setup shown in Figures 4D and 4E. The hybrid SOCAL coating is thermally stable up to 230°C,⁵⁶ with no coating thickness reduction or degradation observed after 5 h of a continual jet fuel fouling experiment. Therefore, although more studies are needed, the hybrid SOCAL is a potential candidate as an anti-fouling coating for high-temperature applications.

Deposition of foulant materials inside a heat exchanger will reduce the overall thermal performance. Therefore, the heat exchanger needs to be oversized so it can

provide a temperature difference in the desirable range even with deposition. [Figure S6](#) shows results for the required increase in the heat exchanger size due to deposition to keep the same temperature difference across the heat exchanger.

Coating durability is an important factor for application implementation.⁵⁷ Nanoindentation tests on hybrid coatings revealed a coating hardness value of approximately 1.4 GPa and an elastic modulus of 21.7 GPa.⁵⁸ These values are approximately 10 times higher than commonly used low surface energy polymeric materials such as polytetrafluoroethylene⁵⁹ or polystyrene.⁶⁰ Furthermore, mechanical and chemical stabilities of the coating have been investigated through abrasion and corrosion tests. The hybrid coating remained unchanged after 100 cycles of abrasion tests with a moderate abrasant (CS8) with 1 N load demonstrating higher wear resistance when compared with liquid-infused surfaces (LIS). The corrosion resistance of the coating was investigated through electrochemical polarization tests in a 3 wt % NaCl solution. The corrosion current on the hybrid SOCAL surface was only 0.17 $\mu\text{A}/\text{cm}^2$, which is 18 times smaller when compared with the LIS surface. Therefore, the hybrid SOCAL is chemically stable in mild corrosive media when compared with LIS and bare surfaces. Details of the abrasion and corrosion tests are available in previous work.⁵⁸

In conclusion, we developed a scalable hybrid SOCAL coating capable of mitigating fuel fouling. We use the coating to demonstrate successful autoxidation fouling reduction in a custom experimental internal flow arrangement. We show that the hybrid SOCAL coating reduces fouling due to its ultra-low surface energy and ultra-smooth surface topology. We characterized the fouling morphology and chemistry using optical imaging, FIB milling, electron microscopy, and X-ray spectroscopy analysis. The hybrid SOCAL coating demonstrates unprecedented advantages when compared with bare copper or SS, showing 96% and 97% reduction in fouling rates on copper and SS, respectively. Furthermore, our hybrid coating is on a par or better than commercially available reference coatings and materials, including alumina ceramic and SilcoKlean silicon dioxide. The mechanistic understanding as well as coating method developed here has significant potential for mitigation of other fouling, deposition, and accretion scenarios, including scaling, biofouling, coking, icing, and frosting for a plethora of industries, such as chemical processing, petrochemical installations, desalination systems, power plants, steam generators, building energy technologies, bio devices and sensors, and many more.

EXPERIMENTAL PROCEDURES

Resource availability

Lead contact

Further information and requests for resources and materials should be directed to and will be fulfilled by the lead contact, Nenad Miljkovic (nmiljkov@illinois.edu).

Materials availability

This study did not generate new unique materials.

Data and code availability

Details about the model implementation and the data used in this study can be found in article and the [supplemental information](#). Requests for further information should be directed to the [lead contact](#).

Sol-gel SiO₂ coating

The silicon dioxide (SiO₂) coating is made by utilizing a previously developed dip-coating method,^{61,62} with several alterations to reduce the roughness of the surface

and to reduce the thickness of the SiO₂ layer. A detailed recipe of the sol-gel SiO₂ coating and its properties can be found in our previous work.³⁴ In brief, the sample tubes were first cut to their appropriate size. We used 20.3 cm (8") long, 6.35 mm (1/4") outer diameter (OD) tubes having a 4.7 mm (0.185") inner diameter (ID). The tube length was chosen so that it enabled hydrodynamically and thermally fully developed flow while keeping a balance between the pressure drop, temperature variation across the tube, and the required flow rate to be compatible with the JFTOT standard. The tube metals used were copper (no. 8967K88, McMaster) and SS (AISI 304, no. 89895K724, McMaster). Both the Cu and SS 304 samples were cleaned by submerging them into a 15 wt % hydrochloric acid (CAS number: 7647-01-0, Sigma-Aldrich) solution, followed by rinsing in deionized (DI) water and isopropanol (IPA) (CAS number: 67-63-0, Sigma-Aldrich), and finally drying in a clean stream of nitrogen gas (N₂).

The sol-gel solution was made by mixing a 1:2.5 molar ratio of tetraethyl orthosilicate (TEOS) (CAS number: 78-10-4, Sigma-Aldrich) and trimethoxymethylsilane (CAS number: 1185-55-3, Sigma-Aldrich). Next, we made a mixture of ethanol (CAS number: 64-17-5, Sigma-Aldrich), DI water, and sodium hydroxide (CAS number: 1310-73-2, Sigma-Aldrich) with a molar ratio of 12.5:17.1:1.1. The amount of ethanol needed was determined by the required molar ratio to TEOS of 3:1. After making the solvent mixture, the solvent was gradually added to the silane mixture. During the process, a stir bar was used to mix solvent and silane, rotating at the rate of 200–250 rpm. After adding the solvent, the beaker was capped. During mixing, a large amount of heat is released, hence an abundant amount of ice is needed in the ice bath to absorb the energy and keep the temperature constant. Stirring was allowed to continue for at least 10 min or until the solution was cooled back down to below 5°C. Considering the large amount of heat generated, the total amount of solution was limited to batches of 150 mL according to the size of our sample.

The dip-coating procedure was controlled by a linear motor (PA-18, Progressive Automations) energized with a power supply (E3631A, Keysight) to maintain constant dipping and withdrawal speeds (Figure 4A). In this work, a constant dipping speed of 15 cm/min was used with a withdraw speed of 15 cm/min. After withdrawal, the tube samples were set against a vertical surface, so all sides were exposed to the laboratory air, allowing drying at room temperature typically within 10 min of removal. Following the sol-gel coating, the samples were sintered in a tube furnace (Lindberg/BlueM Moldatherm Box Furnace) filled with N₂ at 500°C for 30 min to sinter the porous sol-gel coating and hence reduce roughness (Figure 4B). See Note S2 and Tables S3 and S4 for surface composition analysis of the Cu and SS 304 substrates coated with sol-gel SiO₂.

SOCAL coating

The SOCAL coating methodology was adopted from previous work.⁶³ The detailed recipe and procedure of SOCAL coating used herein can be found in our previous work.³² In brief, SOCAL was made by mixing 100:20:1 wt % IPA (CAS number: 67-63-0, Sigma-Aldrich), dimethyldimethoxysilane (CAS number: 1112-39-6, Sigma-Aldrich) and sulfuric acid (CAS number: 7664-93-9, Sigma-Aldrich). After stirring the mixture, the solution was allowed to rest in a capped glass container for at least 20 min before use.

Metal tube samples coated with the sol-gel SiO₂ coating were cleaned by a mixture of 100:1 wt % IPA (CAS number: 67-63-0, Sigma-Aldrich) and sulfuric acid (CAS

number: 7664-93-9, Sigma-Aldrich). The solution reacts off sodium hydroxide residue on the sol-gel coating. The metal sample was immersed in the cleaning solution for 10 s. Immediately after, while the sample was still wet, the sample was submerged in the quiescent SOCAL solution for 5–10 s and withdrawn gradually at a rate of ≈ 2 cm/s by hand. After removal, the sample was allowed to reside at room temperature for 20 min to ensure complete drying (Figure 4C). Next, the sample was cleaned again using vigorous rinsing for 10 s each in DI water, IPA, toluene (CAS number: 108-88-3, Sigma-Aldrich), and again IPA. Finally, the sample was blown dry with a clean N₂ stream.

SilcoKlean coating

The SilcoKlean 1000 coating was done by SilcoTek. According to SilcoTek, SilcoKlean 1000 is a CVD layer, designed specifically to reduce coking of steel, SS, and specialty alloys (https://www.silcotek.com/hubfs/docs/SilcoKlean_Data_Sheet.pdf). The deposition method utilized a non-line-of-sight CVD process to produce a flexible, amorphous silicon layer that diffuses into the metal lattice and conforms to intricate surfaces while maintaining high-dimensional tolerances. The surface of the amorphous silicon has a layer of silicon dioxide reported by element analysis. The substrate metal needs to be an anti-corrosive alloy. Metals, such as copper and aluminum, cannot be coated, hence the SilcoKlean 1000 coating was only applied to the SS 304 tube samples.

Jet fuel fouling experiments

To analyze the fuel fouling behavior of the internally coated tubes, a customized jet fuel fouling test rig was designed and built. The test setup and procedure were based on the JFTOT, but did not mimic all conditions of JFTOT. For the test, the base Cu and bare SS tubes, as well as their hybrid SOCAL-coated counterparts, are inserted in the test apparatus. In addition to these samples, alumina ceramic (8746K372, McMaster) (OD = 6.35 mm, ID = 4.7 mm, and length = 20.3 cm) and Inconel 600 (3ACP4, Grainger) (OD = 6.35 mm, ID = 4.6 mm, and length = 20.3 cm) as well as SS tubes coated with SilcoKlean 1000 (SilcoTek) (OD = 6.35 mm, ID = 4.7 mm, and length = 20.3 cm) were also characterized in the setup to benchmark performance. The alumina sample was included due to past experiments showing reduced jet fuel fouling on alumina-coated substrates.⁵¹ The Inconel 600 sample was included due to its prevalent use as a manufacturing material in the aerospace industry.^{29,49,50} The SilcoKlean 1000 coating was rationally selected as it represents a commercially available coating that was developed for jet fuel fouling mitigation.

A block diagram of the experiment arrangement is shown in Figure 4D. The test was conducted in an SS (SS 304, McMaster) pool filled with silicone oil (poly(dimethylsiloxane-co-methylphenylsiloxane), CAS number: 63148-52-7, Sigma-Aldrich). An immersive heater (1489N38 1 kW, McMaster) and a proportional integral differential controller (EZ Zone PM3J1CA, Watlow) was used to control the temperature of the pool. Immersion heating of the pool was used to ensure a homogeneous temperature environment for the Jet-A fuel passing through the tube samples. Furthermore, the use of a heating liquid pool allowed for the creation of an oxygen-reduced environment in the case of a leak forming and jet fuel vaporizing and escaping the test sample section of the flow loop. Finally, immersion heating enabled easy observation of any gaseous leak as bubbles would form at the leak site. The jet fuel was pumped by a peristaltic pump (HV-77122, MasterFlex) from a 2 gallon fuel-safe reservoir (4290T151, McMaster). The inlet and outlet temperatures were measured

with two thermocouples (Type T, Omega) fitted to T-sections. The tubes were oriented horizontally for all tests conducted.

After leaving the test section, the jet fuel working fluid is directed into a customized cooling tower to reduce the temperature of fuel for safety. The cooling tower consists of a cooling fan with 31 CFM capacity (9191K29, McMaster), a 3D printed polymer case, and a custom manufactured Cu cooling coil. As shown in [Figure 4](#), cool air was pulled through the 3D printed case to cool down the external surface of the Cu coil as well as the jet fuel flowing inside. Considering the low flow rate of the jet fuel, air cooling was sufficient to cool the jet fuel back to room temperature. At the cooling tower outlet, the jet fuel was then directed to a fuel-safe waste reservoir (4290T151, McMaster). We did not re-circulate the jet fuel to avoid any possibility of contamination buildup and interaction with metals in the flow loop, which has been shown to affect fouling. [Table S1](#) outlines all sensors, spans, and uncertainties of the test setup.

The temperature of the silicone oil in the heating bath was set to 215°C. The safe operating range for the oil was –40°C to 230°C. The flow rate of the fuel was estimated from the peristaltic pump specifications. For a specific diameter of the soft tube in the pump, every cycle sends out a specified volume of liquid. In our setup, a 0.89 mm ID tube was used, with every full rotation pumping 0.024 mL of jet fuel. Our rotation speed of the peristaltic pump was set to 200 rpm; hence, the total flow rate for all experiments was 4.8 ± 0.1 mL/min. The corresponding internal flow Reynolds number was ~ 10.5 . Both the hydrodynamic and thermal entrance length were less than 3 mm long. The connection to the sample was chosen to be 3 cm to ensure that the flow entering the test section is both hydrodynamically and thermally fully developed. See [Note S4](#) for development length calculation details. The test duration was 5.2 h for each sample, and a total of about 1.5 L fuel was used per individual test run. The flow rate was calibrated using a separate method by measuring the time required to fill a 50 mL graduated cylinder. [Table S2](#) shows a breakdown comparison between our test conditions and those of the JFTOT test, which was the guideline we followed during design.

After the experiment was complete, the samples were thoroughly rinsed using a 1:1:1 mixture of acetone, toluene, and IPA, then blown dry using a clean N₂ gas stream. This cleaning step removes any jet fuel residue from inside the samples. The samples were cut axially down the middle for visual inspection, as well as into 1 cm long specimens for further chemical analysis.

FIB milling

To quantify the thickness of the carbon deposit, FIB milling (Scios 2 DualBeam, Thermal Fisher) was utilized on the test specimen. Using ion milling, we were able to cut through the carbon deposit and observe the interface of deposition and metal substrate beneath. FIB milling was done using the middle part of the tube (4" from the inlet and outlet) and at a random spot in the azimuthal direction. Before the FIB milling, a thin layer (<10 nm) of gold was deposited via sputtering on the sample. The gold enables electrical conductivity of the sample, as neither the carbon deposit nor the hybrid SOCAL coating are conductive. Usually, a 20 μm wide and 10 μm deep cross-section was cut for SEM inspection. The ion current was set to 3.5 nA at a voltage to 8 kV. The cutting process took about 13 min for one spot. A cleaning process was used to better determine the interface between carbon deposition and metal tube by reducing the ion current and milling rate. During the cleaning process, the sample was first tilted to 53°, 1° more than the ion milling mode angle. A

20 × 1 μm milling section with 0.7 nA current was aimed at the target wall. This mild ion beam cleans off any residue on the wall caused by high-power ion milling, thus the structure of the interfaces and materials beneath the top layer are revealed. The thickness of carbon deposition was measured at five different spatial locations for each sample.

SEM

Low- and high-resolution field emission scanning electron microscopy (FESEM) images of each sample were obtained using an FEI Quanta 450 ESEM in high-vacuum operation mode. The accelerating voltage was set to 5 kV, and emission current was approximately 30 pA with a spot size of 2 nm to prevent charging and sample damage by the electron beam. Before FESEM, the tube samples were sputter coated with a 5 nm thick layer of Au-Pd. The deposit shape and overall surface topology were characterized by positioning the sample perpendicular to the electron beam (top view) or at a 45° inclined orientation (side view).

XPS

To analyze the composition of the carbon deposition observed with FIB milling and SEM imaging, XPS was used. XPS allowed us to determine the surface elemental composition and percentage. All samples were subjected to a broad survey from 1,100 to 0 eV. Following the survey, finer detailed scans were done at the carbon, oxygen, and silicon peaks at 295–275, 539–519, and 109–92 eV, respectively. All of the data obtained was processed using the free software CasaXPS.

Energy dispersive X-ray spectroscopy

EDS analysis of the sol-gel SiO₂-coated samples (Figure S5) was conducted using the FEI Quanta FEG 450 ESEM. To study the chemical composition of the surfaces, wide band EDS scanning was performed on eight random spots on each sample.

SUPPLEMENTAL INFORMATION

Supplemental information can be found online at <https://doi.org/10.1016/j.xcrp.2022.100859>.

ACKNOWLEDGMENTS

The authors would like to acknowledge the funding and technical support from the Center for Integrated Thermal Management of Aerospace Vehicles (CITMAV). N.M. gratefully acknowledges funding support from the Office of Naval Research (ONR) (grant no. N00014-16-1-2625), the Air Conditioning and Refrigeration Center (ACRC), an NSF funded I/UCRC at UIUC and the International Institute for Carbon-Neutral Energy Research (WPI-I2CNER), sponsored by the Japanese Ministry of Education, Culture, Sports, Science and Technology. J.M. gratefully acknowledges funding support from the PPG Fellowship. Scanning electron microscopy (SEM), X-ray photoelectron spectroscopy (XPS), and focused ion beam (FIB) milling were carried out in the Materials Research Laboratory Central Facilities, University of Illinois.

AUTHOR CONTRIBUTIONS

N.M. conceived the idea. S.K. and H.Z. developed the coating and fabricated the samples. S.K., H.Z., and Q.W. built the experimental setup. S.K., H.Z., K.F.R., and Q.W. conducted the jet fuel fouling experiments. S.K., H.Z., K.F.R., and J.M. conducted surface characterization. H.Z. conducted the image processing using ImageJ. S.K. conducted the thermal analysis. S.K., H.Z., and N.M. conducted the data

analysis. S.K., H.Z., and N.M. wrote the manuscript. N.M. supervised the project. All authors have contributed to editing the manuscript and have given approval to the final version of the manuscript.

DECLARATION OF INTERESTS

The authors declare no competing interests.

Received: May 19, 2021

Revised: February 22, 2022

Accepted: March 28, 2022

Published: April 25, 2022

REFERENCES

- Huang, H., Spadaccini, L.J., and Sobel, D.R. (2004). Fuel-cooled thermal management for advanced aeroengines. *J. Eng. Gas Turbines Power* 126, 284–293. <https://doi.org/10.1115/1.1689361>.
- Butnark, S. (2003). Thermally Stable Coal-Based Jet Fuel: Chemical Composition, Thermal Stability, Physical Properties and Their Relationships. Ph.D. (The Pennsylvania State University).
- Goel, P., and Boehman, A.L. (2000). Numerical simulation of jet fuel degradation in flow reactors. *Energy Fuels* 14, 953–962.
- Ervin, J.S., Heneghan, S.P., Martel, C.R., and Williams, T.F. (1996). Surface effects on deposits from jet fuels. *J. Eng. Gas Turbines Power* 118, 278–285. <https://doi.org/10.1115/1.2816589>.
- Edwards, T. (2006). Cracking and deposition behavior of supercritical hydrocarbon aviation fuels. *Combust. Sci. Technol.* 178, 307–334.
- Yu, J., and Eser, S. (1995). Determination of critical properties (T_c, P_c) of some jet fuels. *Ind. Eng. Chem. Res.* 34, 404–409.
- Edwards, T., and Zabarnick, S. (1993). Supercritical fuel deposition mechanisms. *Ind. Eng. Chem. Res.* 32, 3117–3122. <https://doi.org/10.1021/ie00024a022>.
- Jones, E.G., Balster, L.M., and Balster, W.J. (1995). Quantitative evaluation of jet-fuel fouling and the effect of additives. *Energy Fuels* 9, 906–912.
- Jones, E.G., Balster, W.J., and Balster, L.M. (1997). Aviation fuel recirculation and surface fouling. *Energy Fuels* 11, 1303–1308.
- Hazlett, R.N. (1991). Thermal Oxidation Stability of Aviation Turbine Fuels (Astm International).
- Batts, B., and Fathoni, A.Z. (1991). A literature review on fuel stability studies with particular emphasis on diesel oil. *Energy Fuels* 5, 2–21.
- Morris, R.E., and Turner, N.H. (1990). Influences exerted by metal deactivator on the thermal stability of aviation fuel in the presence of copper. *Fuel Sci. Technol. Int.* 8, 327–350.
- Antonio, E.N., Wicking, C., Filip, S., Ryan, M.P., and Heutz, S. (2020). Role of iron speciation in oxidation and deposition at the hexadecane–iron interface. *ACS Appl. Mater. Interfaces* 12, 19140–19152.
- Waynick, J.A. (2001). The development and use of metal deactivators in the petroleum industry: a review. *Energy Fuels* 15, 1325–1340.
- West, Z.J., Adams, R.K., and Zabarnick, S. (2011). Homogeneous catalysis of liquid-phase hydroperoxide decomposition in hydrocarbons. *Energy Fuels* 25, 897–904.
- Zabarnick, S., and Grinstead, R.R. (1994). Studies of jet fuel additives using the quartz crystal microbalance and pressure monitoring at 140.Degree.C. *Ind. Eng. Chem. Res.* 33, 2771–2777.
- Beaver, B., Rawlings, D., Neta, P., Alfassi, Z., and Das, T. (1998). Structural effects on the reactivity of substituted arylphosphines as potential oxygen-scavenging additives for future jet fuels. *Heteroatom Chem.* 9, 133–138.
- Beaver, B., Sharief, V., Teng, Y., DeMunshi, R., Guo, J., Katondo, E., Gallaher, D., Bunk, D., Grodkowski, J., and Neta, P. (2000). Development of oxygen scavenger additives for future jet fuels. A role for electron-transfer-initiated oxygenation (ETIO) of 1, 2, 5-trimethylpyrrole? *Energy Fuels* 14, 441–447.
- Spadaccini, L.J., and Huang, H. (2002). On-line fuel deoxygenation for coke suppression. pp. 377–383.
- Gül, Ö., Rudnick, L.R., and Schobert, H.H. (2008). Effect of the reaction temperature and fuel treatment on the deposit formation of jet fuels. *Energy Fuels* 22, 433–439.
- Liu, G., Cao, Y., Jiang, R., Wang, L., Zhang, X., and Mi, Z. (2009). Oxidative desulfurization of jet fuels and its impact on thermal-oxidative stability. *Energy Fuels* 23, 5978–5985.
- Jones, E.G., Balster, L.M., and Balster, W.J. (1996). Thermal stability of Jet-A fuel blends. *Energy Fuels* 10, 509–515.
- Jones, E.G., and Balster, L.M. (1999). Autoxidation of dilute jet-fuel blends. *Energy Fuels* 13, 796–802.
- Heneghan, S.P., Zabarnick, S., Ballal, D., and Harrison, W., III (1996). JP-8+ 100: The Development of High-Thermal-Stability Jet Fuel. *Journal of Energy Resources Technology* 118, 170–179. <https://doi.org/10.1115/1.2793859>.
- Ram Mohan, A., and Eser, S. (2011). Effectiveness of low-pressure metal–organic chemical vapor deposition coatings on metal surfaces for the mitigation of fouling from heated jet fuel. *Ind. Eng. Chem. Res.* 50, 7290–7304. <https://doi.org/10.1021/ie1025375>.
- Kondyli, A., and Schrader, W. (2020). Understanding “fouling” in extremely complex petroleum mixtures. *ACS Appl. Energ. Mater.* 3, 7251–7256. <https://doi.org/10.1021/acsaem.0c01326>.
- Gengenbach, T.R., Major, G.H., Linford, M.R., and Easton, C.D. (2021). Practical guides for x-ray photoelectron spectroscopy (XPS): interpreting the carbon 1s spectrum. *J. Vacuum Sci. Technol. A* 39, 013204.
- Yang, C., Liu, G., Wang, X., Jiang, R., Wang, L., and Zhang, X. (2012). Preparation and anticoking performance of MOCVD alumina coatings for thermal cracking of hydrocarbon fuels under supercritical conditions. *Ind. Eng. Chem. Res.* 51, 1256–1263. <https://doi.org/10.1021/ie201978c>.
- Altin, O., and Eser, S. (2001). Analysis of carbonaceous deposits from thermal stressing of a JP-8 fuel on superalloy foils in a flow reactor. *Ind. Eng. Chem. Res.* 40, 589–595. <https://doi.org/10.1021/ie0004489>.
- Altin, O., and Eser, S. (2000). Characterization of carbon deposits from jet fuel on Inconel 600 and Inconel X surfaces. *Ind. Eng. Chem. Res.* 39, 642–645.
- Łodziana, Z., Topsøe, N.-Y., and Nørskov, J.K. (2004). A negative surface energy for alumina. *Nat. Mater.* 3, 289–293.
- Zhao, H., Deshpande, C.A., Li, L., Yan, X., Hoque, M.J., Kuntumalla, G., Rajagopal, M.C., Chang, H.C., Meng, Y., and Sundar, S. (2020). Extreme antiscaling performance of slippery omniphobic covalently attached liquids. *ACS Appl. Mater. Interfaces* 12, 12054–12067.
- Azimi, G., Cui, Y., Sabanska, A., and Varanasi, K.K. (2014). Scale-resistant surfaces: fundamental studies of the effect of surface energy on reducing scale formation. *Appl. Surf. Sci.* 313, 591–599.
- Khodakarami, S., Zhao, H., Rabbi, K.F., and Miljkovic, N. (2021). Scalable corrosion-resistant coatings for thermal applications. *ACS Appl. Mater. Interfaces* 13, 4519–4534. <https://doi.org/10.1021/acsaami.0c19683>.

35. Subramanyam, S.B., Azimi, G., and Varanasi, K.K. (2014). Designing lubricant-impregnated textured surfaces to resist scale formation. *Adv. Mater. Interfaces* 1, 1300068.
36. Cha, H., Vahabi, H., Wu, A., Chavan, S., Kim, M.-K., Sett, S., Bosch, S.A., Wang, W., Kota, A.K., and Miljkovic, N. (2020). Dropwise condensation on solid hydrophilic surfaces. *Sci. Adv.* 6, eaax0746. <https://doi.org/10.1126/sciadv.aax0746>.
37. Meng, J., and Wang, S. (2020). Advanced antiscaling interfacial materials toward highly efficient heat energy transfer. *Adv. Funct. Mater.* 30, 1904796. <https://doi.org/10.1002/adfm.201904796>.
38. Mantel, M., and Wightman, J. (1994). Influence of the surface chemistry on the wettability of stainless steel. *Surf. Interface Anal.* 21, 595–605.
39. Aqra, F., and Ayyad, A. (2011). Surface energies of metals in both liquid and solid states. *Appl. Surf. Sci.* 257, 6372–6379. <https://doi.org/10.1016/j.apsusc.2011.01.123>.
40. Keysar, S., Semiat, R., Hasson, D., and Yahalom, J. (1994). Effect of surface roughness on the morphology of calcite crystallizing on mild steel. *J. Colloid Interface Sci.* 162, 311–319. <https://doi.org/10.1006/jcis.1994.1044>.
41. Vudayagiri, S., Junker, M.D., and Skov, A.L. (2013). Factors affecting the surface and release properties of thin polydimethylsiloxane films. *Polym. J.* 45, 871–878. <https://doi.org/10.1038/pj.2012.227>.
42. Sun, Z., Wen, J., Wang, W., Fan, H., Chen, Y., Yan, J., and Xiang, J. (2020). Polyurethane covalently modified polydimethylsiloxane (PDMS) coating with increased surface energy and re-coatability. *Prog. Org. Coat.* 146, 105744.
43. Zhao, X., Khatir, B., Mirshahidi, K., Yu, K., Kizhakkedathu, J.N., and Golovin, K. (2021). Macroscopic evidence of the liquidlike nature of nanoscale polydimethylsiloxane brushes. *ACS Nano*. 15, 13559–13567. <https://doi.org/10.1021/acsnano.1c04386>.
44. Zhang, L., Guo, Z., Sarma, J., Zhao, W., and Dai, X. (2021). Gradient quasi-liquid surface enabled self-propulsion of highly wetting liquids. *Adv. Funct. Mater.* 31, 2008614. <https://doi.org/10.1002/adfm.202008614>.
45. Kazi, F.R., Jin, Y.H., Xiao, Y., Jingcheng, M., Muhammad, J.H., Soumyadip, S., and Nenad, M. (2022). Polydimethylsiloxane-silane synergy enables dropwise condensation of low surface tension liquids. *Adv. Funct. Mater.* <https://doi.org/10.1002/adfm.202112837>.
46. Zhang, L., Guo, Z., Sarma, J., and Dai, X. (2020). Passive removal of highly wetting liquids and ice on quasi-liquid surfaces. *ACS Appl. Mater. Interfaces* 12, 20084–20095. <https://doi.org/10.1021/acscami.0c02014>.
47. Liu, J., Sun, Y., Zhou, X., Li, X., Kappl, M., Steffen, W., and Butt, H.-J. (2021). One-step synthesis of a durable and liquid-repellent poly(dimethylsiloxane) coating. *Adv. Mater.* 33, 2100237. <https://doi.org/10.1002/adma.202100237>.
48. McDonald, J.C., and Whitesides, G.M. (2002). Poly(dimethylsiloxane) as a material for fabricating microfluidic devices. *Acc. Chem. Res.* 35, 491–499. <https://doi.org/10.1021/ar10110q>.
49. Mohan, A.R., and Eser, S. (2010). Analysis of carbonaceous solid deposits from thermal oxidative stressing of jet-A fuel on iron- and nickel-based alloy surfaces. *Ind. Eng. Chem. Res.* 49, 2722–2730. <https://doi.org/10.1021/ie901283r>.
50. Altin, O., and Eser, S. (2006). Pre-oxidation of Inconel alloys for inhibition of carbon deposition from heated jet fuel. *Oxid. Met.* 65, 75–99. <https://doi.org/10.1007/s11085-006-9002-5>.
51. Symoens, S.H., Olahova, N., Muñoz Gandarillas, A.E., Karimi, H., Djokic, M.R., Reyniers, M.-F., Marin, G.B., and Van Geem, K.M. (2018). State-of-the-art of coke formation during steam cracking: anti-coking surface technologies. *Ind. Eng. Chem. Res.* 57, 16117–16136. <https://doi.org/10.1021/acs.iecr.8b03221>.
52. Pei, X., Hou, L., and Roberts, W.L. (2018). Experimental and numerical study on oxidation deposition properties of aviation kerosene. *Energy Fuels* 32, 7444–7450. <https://doi.org/10.1021/acs.energyfuels.8b01250>.
53. Ma, J., Sett, S., Cha, H., Yan, X., and Miljkovic, N. (2020). Recent developments, challenges, and pathways to stable dropwise condensation: a perspective. *Appl. Phys. Lett.* 116, 260501. <https://doi.org/10.1063/5.0011642>.
54. Mousa, M.H., Yang, C.-M., Nawaz, K., and Miljkovic, N. (2022). Review of heat transfer enhancement techniques in two-phase flows for highly efficient and sustainable cooling. *Renew. Sust. Energy Rev.* 155, 111896. <https://doi.org/10.1016/j.rser.2021.111896>.
55. Mousa, M.H., Miljkovic, N., and Nawaz, K. (2021). Review of heat transfer enhancement techniques for single phase flows. *Renew. Sust. Energy Rev.* 137, 110566.
56. Zhao, H., Deshpande, C.A., Li, L., Yan, X., Hoque, M.J., Kuntumalla, G., Rajagopal, M.C., Chang, H.C., Meng, Y., Sundar, S., et al. (2020). Extreme antiscaling performance of slippery omniphobic covalently attached liquids. *ACS Appl. Mater. Interfaces* 12, 12054–12067. <https://doi.org/10.1021/acscami.9b22145>.
57. Ho, J.Y., Rabbi, K.F., Khodakarami, S., Ma, J., Boyina, K.S., and Miljkovic, N. (2022). Opportunities in nanoengineered surface designs for enhanced condensation heat and mass transfer. *J. Heat Transfer*. <https://doi.org/10.1115/1.4053454>.
58. Zhao, H., Khodakarami, S., Deshpande, C.A., Ma, J., Wu, Q., Sett, S., and Miljkovic, N. (2021). Scalable slippery omniphobic covalently attached liquid coatings for flow fouling reduction. *ACS Appl. Mater. Interfaces* 13, 38666–38679. <https://doi.org/10.1021/acscami.1c08845>.
59. Ma, J., Cha, H., Kim, M.-K., Cahill, D.G., and Miljkovic, N. (2019). Condensation induced delamination of nanoscale hydrophobic films. *Adv. Funct. Mater.* 29, 1905222. <https://doi.org/10.1002/adfm.201905222>.
60. Xie, X., Yang, K., Li, D., Tsai, T.-H., Shin, J., Braun, P.V., and Cahill, D.G. (2017). High and low thermal conductivity of amorphous macromolecules. *Phys. Rev. B* 95, 035406. <https://doi.org/10.1103/PhysRevB.95.035406>.
61. Castro, Y., Ferrari, B., Moreno, R., and Durán, A. (2005). Corrosion behaviour of silica hybrid coatings produced from basic catalysed particulate sols by dipping and EPD. *Surf. Coat. Technol.* 191, 228–235. <https://doi.org/10.1016/j.surfcoat.2004.03.001>.
62. Aparicio, M., Jitianu, A., Rodriguez, G., Degnah, A., Al-Marzoki, K., Mosa, J., and Klein, L.C. (2016). Corrosion protection of AISI 304 stainless steel with melting gel coatings. *Electrochim. Acta.* 202, 325–332. <https://doi.org/10.1016/j.electacta.2015.12.142>.
63. Wang, L., and McCarthy, T.J. (2016). Covalently attached liquids: instant omniphobic surfaces with unprecedented repellency. *Angew. Chem. Int. Ed.* 55, 244–248. <https://doi.org/10.1002/anie.201509385>.